Nanoscale

Accepted Manuscript

This article can be cited before page numbers have been issued, to do this please use: L. Peng, Z. BIAN, W. Zhang, S. Garofalo, D. M. Dhumal, J. Zheng, T. Roussel, E. Laurini, C. Galanakou, C. Lauro, M. Maresca, Y. Xia, D. Zhu, S. Pricl, X. Liu and C. Limatola, *Nanoscale*, 2025, DOI: 10.1039/D5NR03017J.

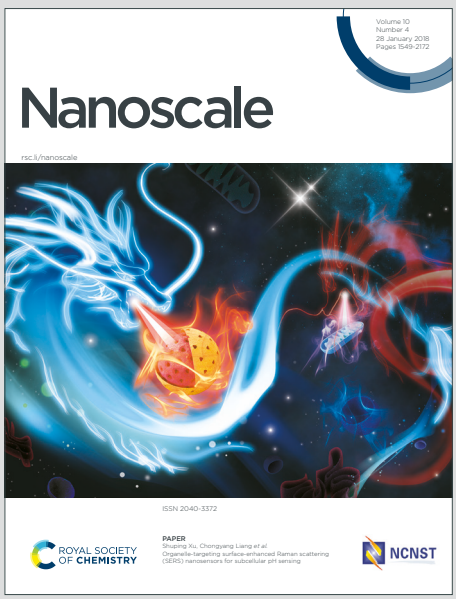

ROYAL SOCIETY OF CHEMISTRY

rsc.li/nanoscale

Bola-amphiphilic glycodendrimers for targeting glial cells in the brain

View Article Online
DOI: 10.1039/D5NR03017J

Zhancun Bian,[1,2] Wenzheng Zhang[2,3], Stefano Garofalo[4], Dinesh Dhumal[2], Junyue Zheng,[1] Tom Roussel[2], Erik Laurini[5], Christina Galanakou,[2] Clotilde Lauro[4], Marc Maresca,[5] Yi Xia[3], Dandan Zhu,[1] Sabrina Pricl[6,7], Xiaoxuan Liu[1,*], Cristina Limatola[4,8], Ling Peng[2,*]

1. State Key Laboratory of Natural Medicines, Joint International Research Laboratory of Target Discovery and New Drug Innovation (Ministry of Education), Jiangsu Key Laboratory of Drug Discovery for Metabolic Diseases, Center of Advanced Pharmaceuticals and Biomaterials, China Pharmaceutical University, Nanjing, P. R. China
2. Aix Marseille University, CNRS, Center Interdisciplinaire de Nanoscience de Marseille, UMR 7325, « Equipe Labellisée Ligue Contre le Cancer », Marseille, France
3. Chongqing Key Laboratory of Natural Product Synthesis and Drug Research, Innovative Drug Research Center, School of Pharmaceutical Sciences, Chongqing University, Chongqing, P. R. China
4. Department of Physiology and Pharmacology, Sapienza University of Rome, Rome, Italy
5. Aix Marseille University, CNRS, Centrale Med, ISM2, 13013 Marseille, France
6. Molecular Biology and Nanotechnology Laboratory (MolBNL@UniTS), DEA, University of Trieste, 34127 Trieste, Italy
7. Department of General Biophysics, Faculty of Biology and Environmental Protection, University of Lodz, 90-236 Lodz, Poland
8. IRCCS Neuromed, Pozzilli, Italy

***Corresponding author:**

Dr Ling Peng

Email: ling.peng@univ-amu.fr

ORCID: 0000-0003-3990-5248

View Article Online
DOI: 10.1039/D5NR03017J

Abstract

Targeting the glial cells in the brain constitutes a formidable challenge due to the presence of the blood-brain barrier (BBB) and the difficulty in achieving specific targeting. Intranasal (IN) administration offers a promising solution to bypass the BBB for delivery directly to the brain, while nanotechnology-based delivery provides tailored targeting capabilities. Here, we report dendrimer-based nanosystems developed for IN administration to target astrocytes and microglia, two types of glial cells that play important roles in maintaining brain homeostasis. Specifically, we demonstrate that bola-amphiphilic glycodendrimers, **Ia** and **Ib**, which bear glucose and mannose terminals, respectively target astrocytes and microglia in mouse brain. These two glycodendrimers, composed of a hydrophobic bola-lipid in the middle connected with two hydrophilic poly(amidoamine) dendrons, were effectively synthesized via click reaction using unprotected carbohydrate building units, and self-assembled into small and spherical nanoparticles by virtue of their amphiphilicity. In a mouse model, both dendrimer nanoparticles successfully reached the brain following IN administration, where the glucose-dendrimer **Ia** selectively targeted astrocytes, and the mannose-dendrimer **Ib** microglia. These findings highlight the potential of glycodendrimer-based nanosystems for precise targeting in the brain and offer a promising perspective for treating central nervous system (CNS) diseases.

Keywords:

dendrimers, microglia, astrocyte, self-assembling, intranasal administration

View Article Online
DOI: 10.1039/D5NR03017J

Introduction

Central nervous system (CNS) diseases pose significant therapeutic challenges due to the presence of the blood-brain barrier (BBB), the complexity of brain pathologies and the difficulty of delivering drugs effectively to desired glial cells in specific brain regions.[1,2] Astrocytes and microglia are two types of glial cells that play important roles in maintaining brain homeostasis, and many CNS disorders are closely linked to the dysfunction of these glial cells.[3,4] Specifically, astrocytes support neuronal function, regulate synaptic activity, and maintain the integrity of the BBB,[5,6,7] while microglia serve as the brain's primary immune cells, orchestrating inflammatory responses and tissue repair.[4,8] Targeting astrocytes and microglia or modulating their activity presents a promising therapeutic approach, but remains a major challenge due to the restrictive nature of the BBB and the lack of cell-specific targeting strategies.[8,9,10,11]

Intranasal (IN) administration has emerged as a non-invasive and efficient strategy to bypass BBB by delivering therapeutics directly to the brain via the olfactory and trigeminal nerve pathways.[12] This approach avoids systemic circulation, enhances CNS targeting, and minimizes peripheral side effects, making it particularly attractive for tackling CNS disorders.[13] To further improve the efficiency and specificity of IN delivery, nanotechnology-based drug delivery systems have been developed for administration via the IN route.[14,15,16] Nanoparticulate drug formulations have been shown to improve drug stability, prolong drug residence time in the nasal cavity and enhance drug penetration across the nasal mucosa.[14] Most importantly, nanoparticles decorated with targeting ligands have enabled precise targeting and drug delivery to specific regions and cells in the brain, further improving therapeutic outcomes.[14,15,16] For example, insulin-functionalized nanoparticles leverage insulin receptor overexpression in hippocampal neurons to achieve region-specific targeting and delivery of protein drugs, raising therapeutic efficacy for neurodegenerative diseases.[17] Also, nanoparticles functionalized with glucose or mannose units have been investigated to enhance specific delivery and targeting respectively to astrocytes via the glucose transporter 1 (GLUT1)[18,19] or activated microglia via mannose receptors.[20,21] Such specific targeting using nanotechnology-based drug delivery thus provides new therapeutic options for treating CNS disorders.

Dendrimers are a special class of precision nanomaterials that are highly valuable for nanotechnology-based delivery to the CNS by virtue of their unique well-defined dendritic structure and cooperative multivalency confined within a nanoscale 3D architecture.[22,23,24] In particular, amphiphilic dendrimers, composed of distinct hydrophobic and hydrophilic entities, are able to self-organize into nano-assemblies [25,26,27] capable of encapsulating and delivering various pharmaceutical agents, including

View Article Online
DOI: 10.1039/D5NR03017J

anticancer drugs,[28,29,30] nucleic acid therapeutics[31,32] and bioimaging agents.[33,34,35] Specifically, bola-amphiphilic dendrimers consist of two hydrophilic dendrons connected by a hydrophobic "bola-lipid" core scaffold.[31,36,37,38] This design was inspired by the bola-amphiphiles found in extremophile archaea, which possess a unique bola-lipid monolayer membrane structure and exhibit robust tolerance to extreme conditions such as high temperature, acidity and salinity, *etc*.[39] All these features have been successfully harnessed for robust and efficient drug delivery.[31,36,37,38]

We have recently developed bola-amphiphilic glycodendrimers **Ia** and **Ib** (Figure 1A) functionalized with glucose and mannose terminals to target astrocytes and microglia, respectively.[40] The multiple carbohydrate units on the dendrimer surface enhance binding affinity and selectivity through the multivalent cooperative glycoside cluster effect, a mechanism observed in the interaction between glycans and glycoproteins in nature.[41,42] Additionally, the "bola-lipid" chain in **Ia** and **Ib** is shorter than the membrane bilayer, preventing their potential anchoring to the cell membrane. Here, we extended these findings to an in vivo mouse model to evaluate the ability of these two glycodendrimers to reach and selectively target glial cells following IN administration.

Notably, we also introduced an optimized synthetic route for **Ia** and **Ib** to enhance efficiency and yield. Our previous method involved using protected carbohydrates that carry azido functionalities for conjugation with the alkynyl-bearing dendrimer **II** via click reaction (Figure 1B, left). The resulting dendrimers required a tedious and challenging purification process, along with the subsequent removal of the protecting groups. This made the synthesis particularly time-consuming and labor-intensive, as well as compromising product yield. To overcome these drawbacks, we elaborated a new and a more efficient synthesis route using unprotected carbohydrate units, which significantly simplified the purification procedure and improved overall yields (Figure 1B, right). We present herein this novel synthetic approach for preparing the bola-amphiphilic glycodendrimers **Ia** and **Ib**, and the effective targeting of these two dendrimers to astrocytes and microglia, respectively, in mouse brain following IN administration. This study highlights the promise of glycodendrimers as tools for the precision targeting of glial cells, offering a novel strategy of modulating glial cell activity for treating CNS disorders.

View Article Online
DOI: 10.1039/D5NR03017J

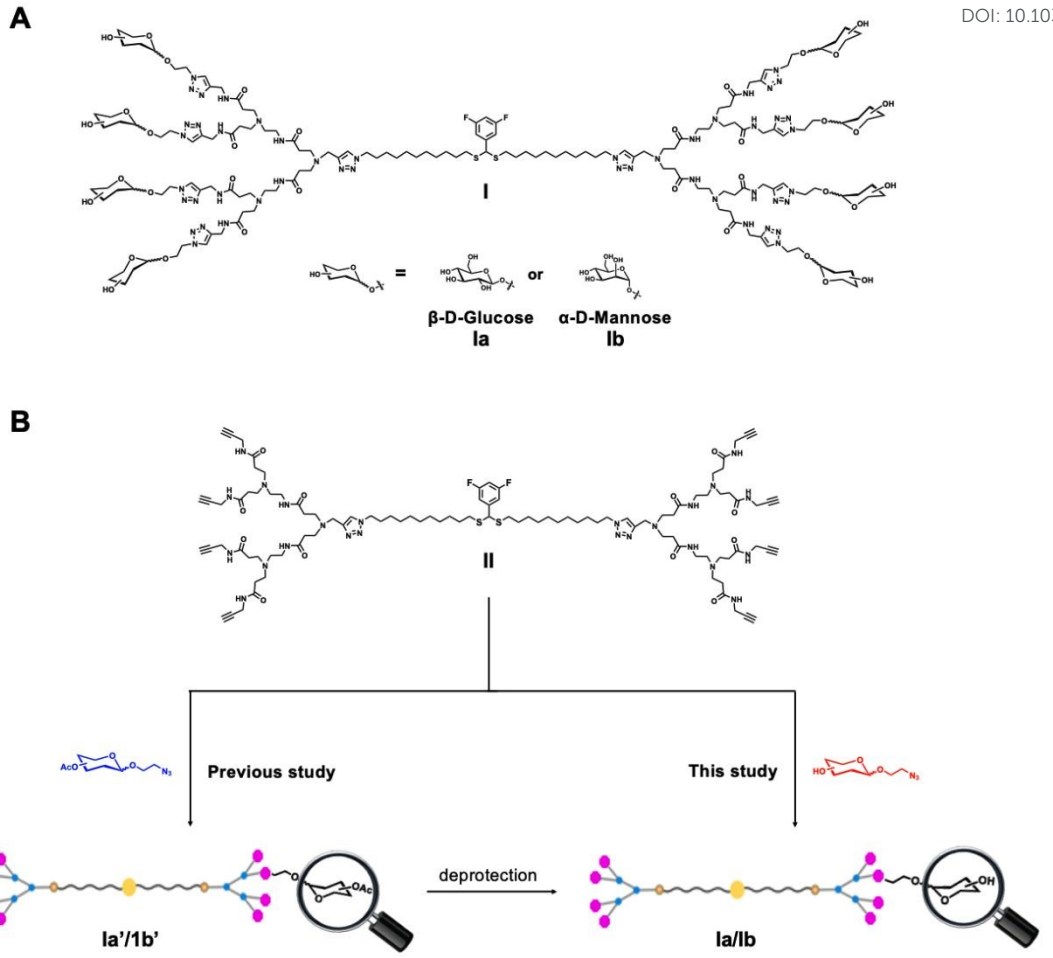

Figure 1. (A) Bola-amphiphilic glycodendrimers, **Ia** and **Ib**, bearing glucose- and mannose-terminals for specifically targeting astrocytes and microglia, respectively, in brain. (B) Synthetic strategies for the bola-amphiphilic dendrimers **Ia** and **Ib** using protected carbohydrate building units in previous study (left) and unprotected carbohydrate units in this study (right).

Results and discussion

Reliable and simplified synthesis of glycodendrimers

The synthesis of both **Ia** and **Ib** started with the alkyne-terminated dendrimer **II**, the precursor for click chemistry conjugation (Figure 1B). We previously prepared **II** by condensing the carboxylic acid-terminated dendrimer **III** with propargylamine in DMF using EDCI and HOBt, along with molecular sieves as a drying agent (Figure 2).[40] However, that approach produced inconsistent yields, ranging from 0 to 81%. To address this issue, we added DIPEA as an auxiliary base to activate the carboxylic acid terminals for reaction with EDCI, while also neutralizing the generated hydrogen chloride to promote the reaction. To further optimize the process, we replaced the high-boiling-point solvent DMF with THF as the solvent, thereby avoiding the time-intensive preparation of anhydrous DMF and its removal during work-up. Collectively,

these adjustments rendered the coupling reaction particularly efficient, consistently yielding the alkyne-terminated dendrimer **II** at stable yields exceeding 75% even without the use of molecular sieves. This greatly simplified the synthesis and purification processes.

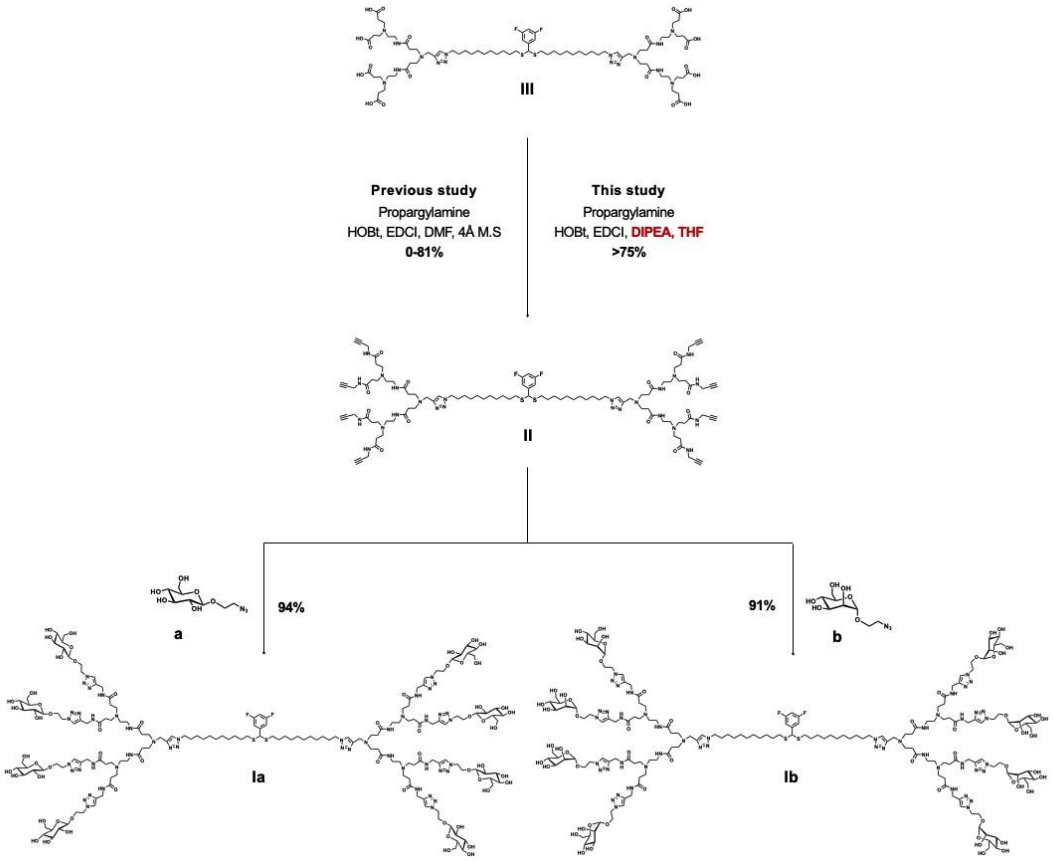

Figure 2. Synthetic methods for alkyne-terminated bola-amphiphilic dendrimer (**II**) and bola-amphiphilic glycodendrimers **Ia** and **Ib.**

We then conjugated the alkyne-terminated dendrimer **II** with unprotected carbohydrate derivatives bearing azido groups via click chemistry to obtain glycodendrimers **Ia** and **Ib**, respectively (Figure 2). The click reaction between **II** and **a** proceeded efficiently in the presence of $CuSO_4 \cdot 5H_2O$ and sodium ascorbate, despite challenges associated with multi-site reactions and steric hindrance of multiple glucose units at the terminals. In addition, **Ia** was easily and conveniently isolated and purified by employing Chelex® resin to chelate and remove the copper ions, followed by dialysis and Sephadex chromatography to eliminate other impurities from the crude product. Subsequent lyophilization gave the final dendrimer **Ia** as a white solid with an excellent yield exceeding 94%.

Compared to the previous method using the protected glucose derivative **a'** (Figure 3, right), the new approach with the unprotected glucose derivative **a** (Figure 2, left and

View Article Online
DOI: 10.1039/D5NR03017J

Figure 3, left) not only reduced the synthesis time and simplified the purification process but also achieved higher yields. Using the same strategy, we also successfully prepared the mannose-dendrimer **Ib** as a white solid with an outstanding yield of 91% (Figure 2, right). The structural integrity and purity of all synthesized dendrimers were confirmed using ^{1}H-, ^{13}C-, and ^{19}F-NMR spectral analyses, as well as high-resolution mass spectrometry (HRMS) (Figure S1/S2/S3).

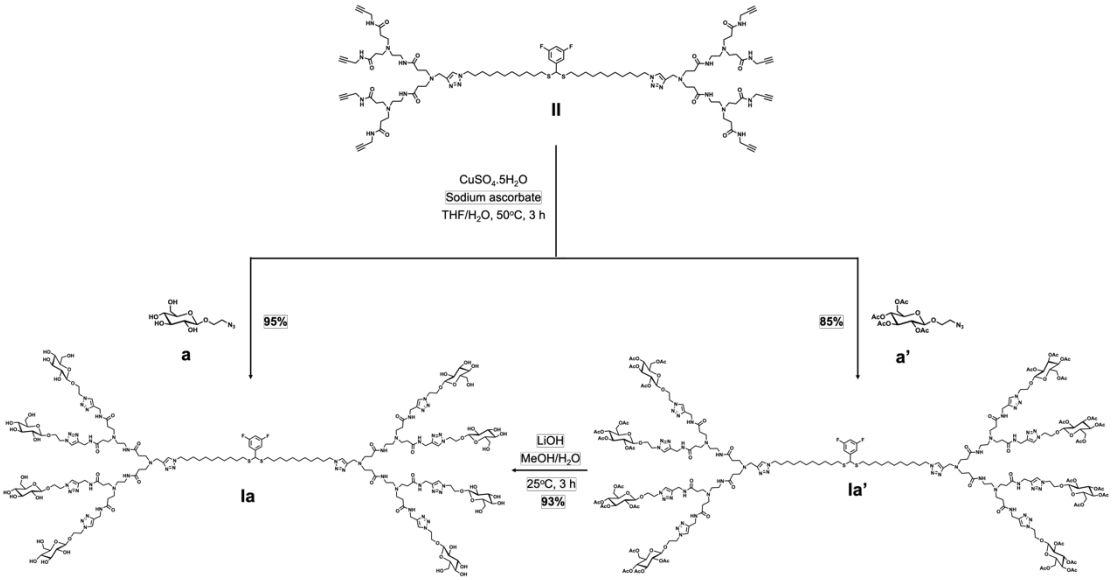

Figure 3. Synthesis of the bola-amphiphilic glucose-dendrimer (**Ia**) using unprotected carbohydrate derivative (left) and protected carbohydrate unit (right).

Self-assembly of glycodendrimers into small, uniform and stable nanoparticles

With the synthesized dendrimers **Ia** and **Ib** in hand, we further studied their self-assembly into nanoparticles in water. Owing to their amphiphilicity, both **Ia** and **Ib** spontaneously formed small nanoparticles (termed as **Ia@** and **Ib@**, respectively) in water, as demonstrated by dynamic light scattering (DLS) analysis (Figure 4A/B). Further transmission electron microscopy (TEM) images of **Ia@** and **Ib@** (Figure 4C/D) confirmed the presence of small, uniform, spherical particles measuring 25±3 nm for **Ia@** and 20±3 nm for **Ib@**, respectively, consistent with the typical characteristics of nanomicelles. In addition, fluorescence spectral analysis revealed similar critical micelle concentrations (CMC) of 34 μM for **Ia@** and 30 μM for **Ib@** (Figure 4E/F). It is also worth noting that both **Ia@** and **Ib@** have slightly positive zeta potentials, +12 mV and +11 mV, respectively (Figure 4G/H), which can help prevent nanoparticle aggregation and may also contribute to minimizing potential toxicity arising from possible interactions with serum proteins or cell membranes, thereby supporting their favorable safety profile reported previously.[40]

View Article Online
DOI: 10.1039/D5NR03017J

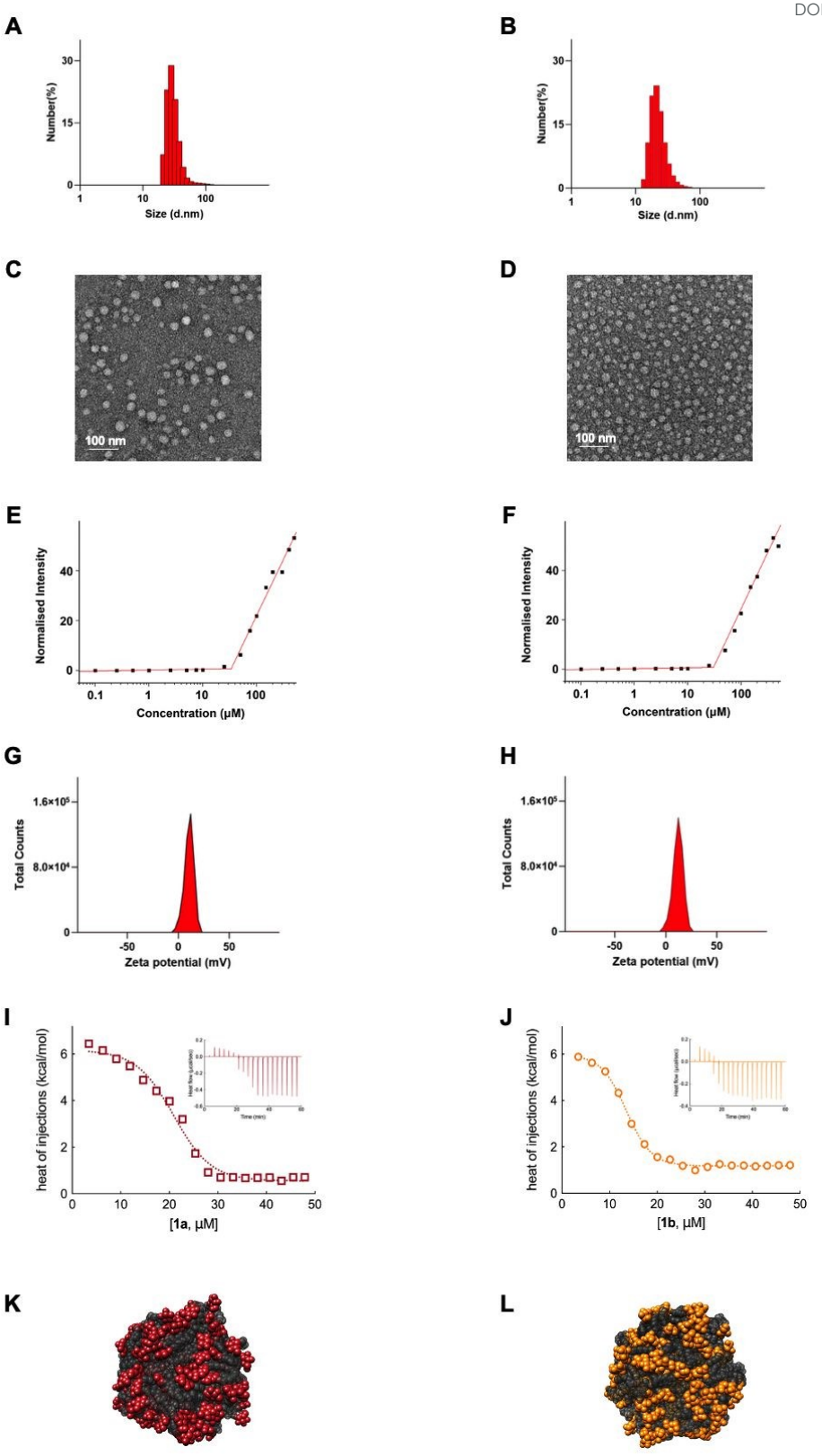

Figure 4. Self-assembly of the bola-amphiphilic glycodendrimers **Ia** and **Ib** into small and uniform nanoparticles, **Ia@** and **Ib@**, respectively. Dynamic light scattering (DLS) analysis of nanoparticles (A) **Ia@** and (B) **Ib@**, respectively, showing their size and size distribution; Transmission electron microscope (TEM) image of (C) **Ia@** and (D) **Ib@** (scale bar 100 nm),

View Article Online
DOI: 10.1039/D5NR03017J

demonstrating their uniform small nanoparticle morphology; Critical micelle concentration measured using fluorescence spectral analysis with Nile Red for (E) **Ia@** and (F) **Ib@**, respectively. Zeta-potential analysis of (G) **Ia@** and (H) **Ib@**, respectively. Representative ITC profiles for the demicellization process of (I) **Ia@** and (J) **Ib@** in water. The dotted lines represent the data fitting with a sigmoidal function, and the insets display the corresponding ITC raw thermograms. Zoomed snapshots from the equilibrated MD trajectory of (K) **Ia@** and (L) **Ib@**.

We next employed isothermal titration calorimetry (ITC) to elucidate the thermodynamic parameters governing the self-assembly and micellization of dendrimers **Ia** and **Ib** following a well-validated procedure.[43,33] The demicellization thermograms for both dendrimers exhibited comparable profiles, indicating similar micellization behaviors (Figure 4I/J). For **Ia**, the CMC was determined to be 21 μM, while **Ib** exhibited a slightly lower CMC of 16 μM. These values are consistent with the data obtained from the fluorescence assay. The standard Gibbs free energy of micellization (ΔG_{mic}) was calculated using the following relationship:

$$\Delta G_{mic} = RT \ln (CMC')$$

where R is the universal gas constant (1.987 cal/mol·K), T is the absolute temperature in Kelvin and CMC' is the critical micellization concentration expressed in molar units. The calculated ΔG_{mic} values were −8.78 kcal/mol for **Ia@** and −8.96 kcal/mol for **Ib@**, indicating a spontaneous micellization process for both bola-amphiphilic dendrimers. The enthalpy change of micellization (ΔH_{mic}) was obtained directly from the ITC measurements, yielding values of −5.31 kcal/mol for **Ia@** and −4.90 kcal/mol for **Ib@**, indicative of an exothermic process. The entropy change ($T\Delta S_{mic}$) associated with micellization was derived from the Gibbs-Helmholtz equation:

$$T\Delta S_{mic} = \Delta H_{mic} - \Delta G_{mic}$$

Consequently, the $T\Delta S_{mic}$ values were calculated to be 3.47 kcal/mol for **Ia@** and 4.06 kcal/mol for **Ib@**, indicative of an increase in system entropy upon micellization. This characteristic is due to the release of structured water molecules from the hydration shells of the hydrophobic tails as the dendrimers aggregate into micelles. Such thermodynamic parameters suggest a combined enthalpic- and entropic-driven micellization. The enthalpy change, arising from favorable interactions between the hydrophilic head groups and the solvent, as well as cooperative packing within the poly(amidoamine) dendrons, plays a key role in micelle stabilization. Simultaneously, the positive entropy values support the notion of increasing disorder associated with water molecule displacement rendering the system thermodynamically favorable. This combination of enthalpic and entropic factors underscores the efficient self-assembly of both dendrimers into stable micellar structures. In summary, ITC analysis

demonstrated that both glucose- and mannose-dendrimers undergo spontaneous, exothermic micellization with comparable thermodynamic parameters and mechanisms driven by a combination of enthalpic stabilization and entropic favorability.

We also examined the nanomicellar formation of both dendrimers using atomistic molecular dynamics (MD) simulations by employing a robust computational protocol.[44,45,46] Starting from a randomized distribution of 22 molecules in solution, the MD simulations resulted in stable micellar nanoassemblies, as depicted in Figure 4K/L. The average micelle gyration radii (R_g) were determined to be approximately 6.8 ± 0.3 nm for **Ia@** and 6.6 ± 0.2 nm for **Ib@** (Figure S4, in Supplementary information), demonstrating high consistency between the two systems and aligning well with the data obtained with the experimental techniques DLS and TEM. The similarity in R_g values suggests that both micelles achieve comparable structural stability and compaction in aqueous environments. A detailed conformational analysis of the micellar architectures, coupled with radial distribution function (RDF) analysis, revealed the spatial organization of the terminal carbohydrate moieties and the hydrophobic core components (Figure S4, in Supplementary information). Both **Ia@** and **Ib@** feature terminal carbohydrate residues that are predominantly exposed on the micellar surface. This structural arrangement ensures their accessibility and the ability to interact effectively with biological targets. The presentation of glucose or mannose residues at the micellar periphery supports their potential recognition by specific biomolecular counterparts, reinforcing their potential functional roles in targeted interactions. Moreover, the same RDF analysis revealed that the hydrophobic regions of both micelles remain primarily concentrated toward the micellar core, effectively shielded from the solvent, as shown by the corresponding RDFs. Despite minor differences in the orientation of the terminal moieties, the micellar structures of **Ia@** and **Ib@** remain highly comparable, achieving an optimal surface presentation of their functional groups, which is critical for their respective biological interactions. In short, ITC and MD simulations together confirm that both systems exhibit robust self-assembly behavior and form stable micellar architectures in solution.

Favorable safety profile and biocompatibility

For delivery to the brain via IN administration, the safety of nanoparticles is an important consideration. As we already assessed the cytotoxicity of **Ia@** and **Ib@** on human embryonic kidney cells (HEK293), mouse fibroblast cells (L929), and Madin-Darby canine kidney cells (MDCK) in our previous study,[40] we therefore focused, in this investigation, the cytotoxicity evaluation on primary human nasal epithelial cells (hNEpCs), microglial BV2 cells, astrocyte C8-D1A cells, mouse brain endothelial bEnd.3 cells and neurons derived from N2a cells using the MTT assay (Figure 5A).

View Article Online
DOI: 10.1039/D5NR03017J

Both **Ia@** and **Ib@** showed no significant cytotoxicity on all tested cells, even at concentrations up to 100 μM, highlighting excellent in vitro biocompatibility.

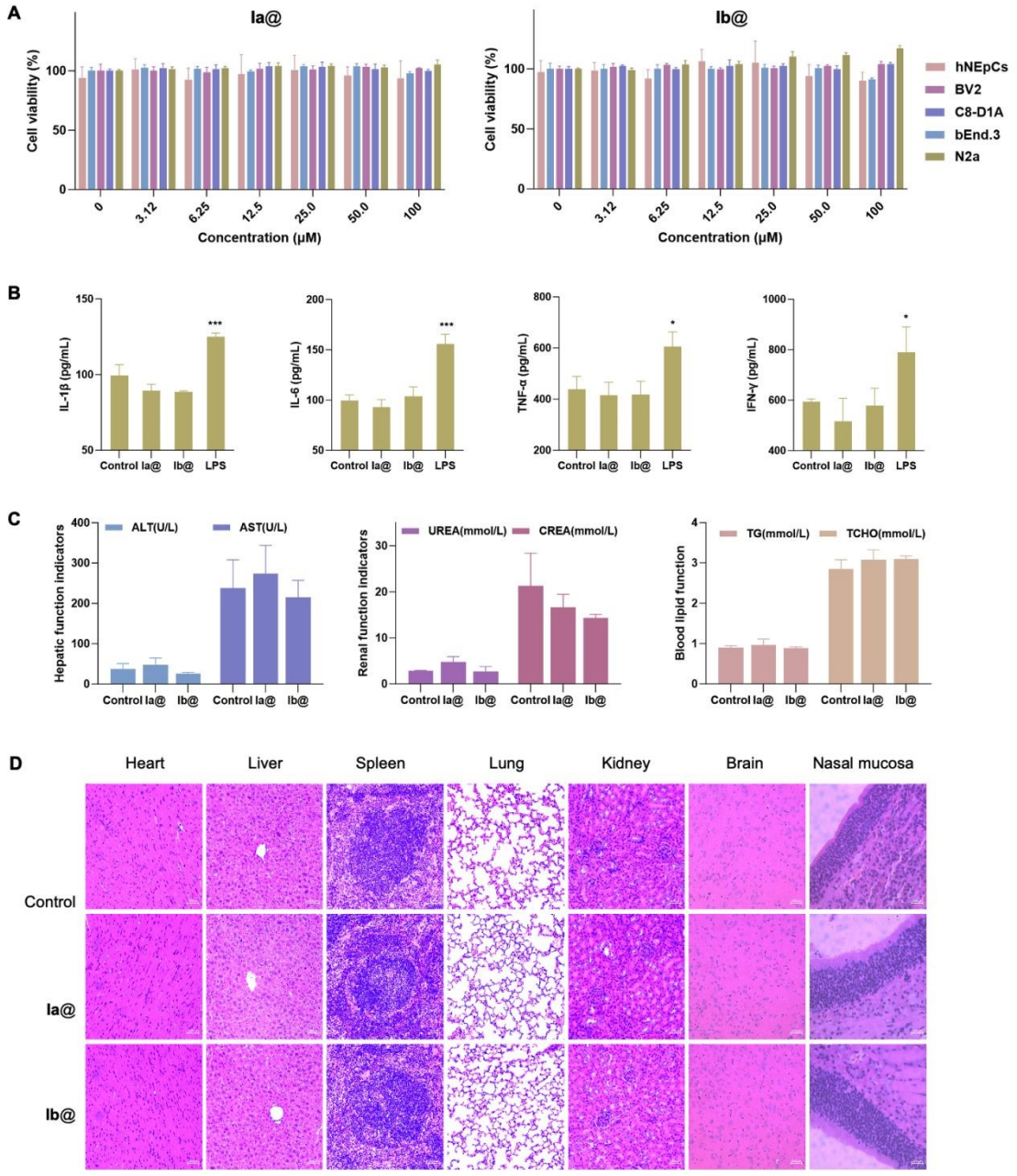

Figure 5. Safety evaluation of **Ia@** and **Ib@**. A) In vitro toxicity evaluation of **Ia@** and **Ib@** on primary human nasal epithelial cells (hNEpCs), microglial BV2 cells, astrocyte C8-D1A cells, mouse brain endothelial bEnd.3 cells and neurons derived from N2a cells in a dendrimer concentration range of 0 to 100 μM at 24 h post-treatment using the MTT assay. (B/C/D) In vivo toxicity evaluation of **Ia@** and **Ib@** in healthy mice (n = 3 for each group of mice). (B) Quantification of the major inflammatory cytokines in serum IL-1β, IL-6, TNF-α, and INF-γ. (C) Liver and kidney function as well as blood lipid by quantifying the levels of biomarkers ALT, AST, UREA, CREA, TCHO and TG in serum. *$p \leq 0.001$, ***$p \leq 0.001$, significance was determined using one-way ANOVA (mean ± SD, n = 3) . (D) Histological analysis of tissues from major organs. Mice were intranasal administrated with PBS, **Ia@** and **Ib@**. Scale bar,

View Article Online
DOI: 10.1039/D5NR03017J

100 μm.

We further assessed the safety profile of **Ia@** and **Ib@** in healthy mice upon intranasal administration, through analysis of inflammatory responses, blood biochemistry, and histopathological changes in major organs. As shown in Figure 5B, no inflammation was observed in healthy mice following treatment with **Ia@** and **Ib@**, compared to the negative control group treated with PBS buffer. In contrast, mice administrated with lipopolysaccharide (LPS) as a positive control exhibited markedly elevated levels of proinflammatory cytokines IL-1β, IL-6, TNF-α, and IFN-γ. Moreover, the kidney function-related parameters (urea and creatinine), liver enzymes (alanine aminotransferase (ALT) and aspartate aminotransferase (AST)), and blood lipid parameters (triacylglycerol (TG) and total cholesterol (TCHO)) remained within normal ranges following intranasal administration of **Ia@** and **Ib@** (Figure 5C), indicating an absence of hepatotoxicity or nephrotoxicity. Also, histological analysis using hematoxylin and eosin (H&E) staining revealed normal tissue architecture and cellular morphology in major organs of mice treated with **Ia@** and **Ib@**, suggesting no discernible pathological abnormalities compared to the PBS-treated control group (Figure 5D). Collectively, these findings indicate that both **Ia@** and **Ib@** exhibit a favorable safety profile, highlighting their potential as candidates for subsequent in vivo studies targeting astrocytes and microglia in the brain.

Effective uptake in brain and specifical target to glial cells

As we already demonstrated **Ia** and **Ib** to target primary cell cultures of astrocytes and microglia, respectively, in our previous in vitro study,[40] we concentrated, in this investigation, on the examination of these two dendrimers to reach the brain and to specifically target astrocytes and microglia in animals using healthy mouse as the animal model.

To facilitate the tracking of brain targeting and uptake, we loaded the nanomicelles **Ia@** and **Ib@** formed by the two dendrimers with the fluorescent dye Cy3, thereafter referred to as Cy3/**Ia@** and Cy3/**Ib@**, respectively. Notably, both Cy3/**Ia@** and Cy3/**Ib@** showed similar size and surface charges to their corresponding non-labelled counterpart **Ia@** and **Ib@** (Figure S5 in Supplementary information), highlighting their relevance to mimic **Ia@** and **Ib@** for use in studying uptake into the brain as well as specific targeting towards astrocytes and microglia.

We then administered Cy3/**Ia@** and Cy3/**Ib@** respectively to C57BL/6 mice via the IN route to track uptake into the mouse brain (Figure 6). Fluorescence signals from Cy3 were observed in the olfactory bulb, hippocampus and striatum of the mice treated with either Cy3/**Ia@** or Cy3/**Ib@**. It is to mention that the olfactory bulb showed the highest

number of fluorescent cells. This can be easily understandable as the olfactory bulb is the first part in the brain to encounter the agent when using IN administration (Figure 6A).

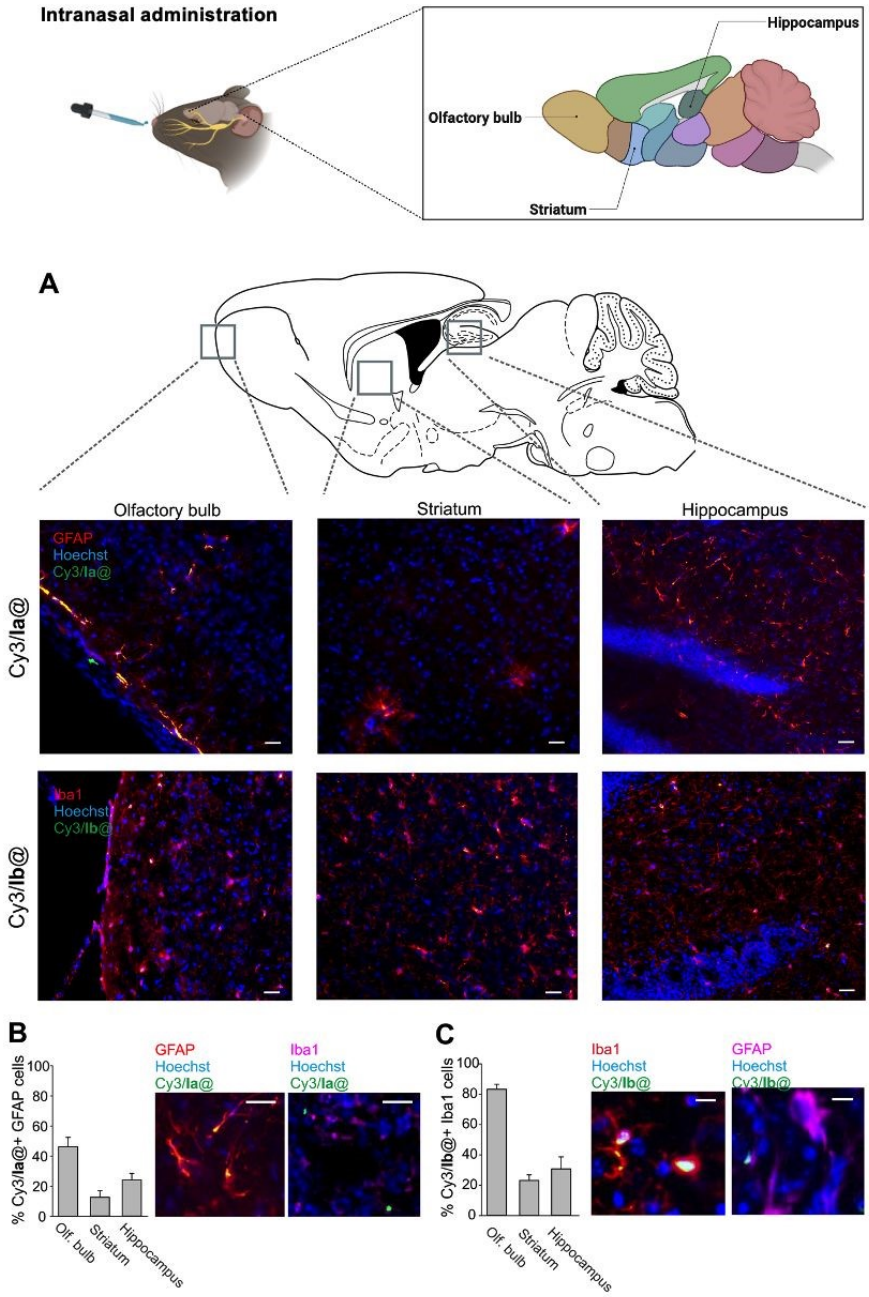

Figure 6: Intranasal administered dendrimer nanoparticles reached mouse brain. (A) Representative immunofluorescence images showing the astrocyte marker Glial Fibrillary Acidic Protein (GFAP; red) and Cy3/**Ia@** (green) (upper panel), and the microglial marker ionized calcium binding adaptor molecule 1 (Iba1; red) and Cy3/**Ib@** (green) (lower panel), Hoechst (blue) to label nuclei, in the transversal section of C57BL/6 mouse brain 24h after intranasal administration of Cy3/**Ia@** and Cy3/**Ib@**, respectively. Scale bar 100 µm. (B) Percentage of Cy3/**Ia@**+ GFAP cells in the olfactory bulb, striatum and hippocampus 24h after intranasal administration of Cy3/**Ia@** (n=5 mice). Right: Representative immunofluorescences

of GFAP (red) or Iba1 (cyan) and Cy3/**Ia@** (green) in the brain of C57BL/6 mice (scale bar 40 μm). (C) Percentage of Cy3/**Ib@**+ Iba1 cells (red) in the olfactory bulb, striatum and hippocampus 24h after intranasal administration of Cy3/**Ib@** (n=5 mice). Right: Representative immunofluorescence of Iba1 (red) or GFAP cells (cyan) and Cy3/**Ib@** (green) in the brain of C57BL/6 mice (scale bar 20 μm).

Further immunohistochemistry analysis revealed co-localization of Cy3/**Ia@** with astrocytes (Figure 6B) and Cy3/**Ib@** with microglia (Figure 6C). No co-localization of Cy3/**Ia@** with microglia (Figure 6B) or Cy3/**Ib@** with astrocytes (Figure 6C) was observed. These findings demonstrate the effective and specific targeting of astrocytes by Cy3/**Ia@**, and microglia by Cy3/**Ib@** within the mouse brain following IN administration. It is noted that single cell analyses revealed a macrophage-specific expression of the mannose receptor, with minor expression in a subset of immature microglia.[47,48] Therefore, the Iba1+ cells co-labeled with Cy3/**Ib@** might also result from the phagocytic activity of microglial cells and/or perivascular macrophage labeling.

Conclusion

In this study, we successfully prepared bola-amphiphilic glycodendrimers bearing glucose and mannose terminals using a simplified synthetic route and evaluated their ability to target specific glial cells in the brain via the IN administration in a mouse model. The novel synthetic strategy, employing unprotected carbohydrate derivatives, provides a more efficient and reliable method for synthesizing glycodendrimers. This new approach reduces the number of synthesis steps and purification procedures while maintaining the structural integrity and purity, as well as achieving higher yields. Further biological evaluation demonstrated that both the glucose dendrimer **Ia** and the mannose dendrimer **Ib** exhibited excellent brain targeting ability, with **Ia** specifically homing in on astrocytes and **Ib** on microglia. Given the emerging therapeutic potential of modulating glial cell activity for treating neurological disorders, glycodendrimers **Ia** and **Ib** therefore hold great promise for translation into drug delivery systems to treat CNS diseases via the simple and non-invasive IN route. Our ongoing research is focused on advancing further along this promising avenue.

View Article Online
DOI: 10.1039/D5NR03017J

Ethical Statement

For intranasal administration, all animal procedures described in the present work were performed in accordance with the guidelines on the ethical use of animals from the European Community Council Directive of September 22, 2010 (2010/63/EU) and from the Italian D.Leg 26/2014., and approved by the Italian Ministry of Health (Authorization N. 78/2017-PR).

For the in vivo toxicity assessment, all animal procedures were approved by the Institutional Animal Care and Use Committee of China Pharmaceutical University, and performed in accordance with the established guidelines and policies for such evaluations (Approval No. YSL-202504091).

Conflicts of interest

The authors declare no competing interests.

Authorship contribution statement

LP conceived and coordinated the project, LP, CL, XL supervised the studies, ZB, WZ, DD, TR performed synthesis and characterization, EL and SP performed ITC and computer modeling, SG, CL, CG, MM, JZ performed the biological evaluation, ZB, WZ, JZ, DZ, DD, TR, SG, CL, CL, LP analyzed the data, ZB, WZ, JZ, DZ, XL, EL, SG, CL, LP wrote the manuscript, all authors read and proofed the manuscript.

Data availability

All data for this study are present in this paper and the Supplementary Materials.

Acknowledgements

This work was funded by the EU Horizon Europe Research and Innovation program Cancer Mission “HIT-GLIO” (2023-2027) (No. 101136835), the French National Research Agency under the frame of the Era-Net EURONANOMED European Research projects “iNanoGUN”, “NANOGLIO”, “TABRAINFEC” and “antineuropatho”, the National Key Research & Development Program of China for

View Article Online
DOI: 10.1039/D5NR03017J

International S&T Cooperation Projects (2018YFE0117800), the Project Program of State Key Laboratory of Natural Medicines (China Pharmaceutical University, No. SKLNMZZ2024JS18), the Ligue Nationale Contre le Cancer (EL2016, EL2021 LNCCLiP), and China Scholarship Council (ZB, WZ). SG was supported by "NextGenerationEU" (DD.3175/2021 E; DD. 3138/2021 CN_3) and National Center for Gene Therapy and Drugs based on RNA Technology (CN 00000041); RF GR-2021-12372494; PRIN 2022 2022488T5S). CL was granted by AIRC (IG2019 23010; MUR: "Progetto ECS 0000024 Rome Technopole, - CUP B83C22002820006, PNRR Missione 4 Componente 2 Investimento 1.5, finanziato dall'Unione europea – NextGenerationEU". EL and SP acknowledge access to supercomputing resources and financial support from ICSC-Centro Nazionale di Ricerca in high-performance computing, big data, and quantum computing (Spoke 7: WP4 (Pilot applications), T.2.8 (Development and optimization of HPC-based integrated workflows based on flagship codes for personalized (nano)medicine); WP5 (Materials Foundry), T.2.3 (Development of computational workflows based on atomistic molecular simulations for the prediction of key properties of molecular system and high-performance (nano)materials for biological, pharmaceutical and industrial application).

References:

(1) Nance, E.; Pun, S. H.; Saigal, R.; Sellers, D. L. Drug Delivery to the Central Nervous System. *Nat. Rev. Mater.* **2021**, *7* (4), 314–331. https://doi.org/10.1038/s41578-021-00394-w.

(2) Zhang, W.; Xiao, D.; Mao, Q.; Xia, H. Role of Neuroinflammation in Neurodegeneration Development. *Signal Transduct. Target. Ther.* **2023**, *8* (1), 267. https://doi.org/10.1038/s41392-023-01486-5.

(3) Brandebura, A. N.; Paumier, A.; Onur, T. S.; Allen, N. J. Astrocyte Contribution to Dysfunction, Risk and Progression in Neurodegenerative Disorders. *Nat. Rev. Neurosci.* **2023**, *24* (1), 23–39. https://doi.org/10.1038/s41583-022-00641-1.

(4) Colonna, M.; Butovsky, O. Microglia Function in the Central Nervous System During Health and Neurodegeneration. *Annu. Rev. Immunol.* **2017**, *35* (1), 441–468. https://doi.org/10.1146/annurev-immunol-051116-052358.

(5) Wu, D.; Chen, Q.; Chen, X.; Han, F.; Chen, Z.; Wang, Y. The Blood–Brain Barrier: Structure, Regulation and Drug Delivery. *Signal Transduct. Target. Ther.* **2023**, *8* (1), 217. https://doi.org/10.1038/s41392-023-01481-w.

(6) Pandit, R.; Chen, L.; Götz, J. The Blood-Brain Barrier: Physiology and Strategies for Drug Delivery. *Adv. Drug Deliv. Rev.* **2020**, *165–166*, 1–14. https://doi.org/10.1016/j.addr.2019.11.009.

(7) Verkhratsky, A.; Butt, A.; Li, B.; Illes, P.; Zorec, R.; Semyanov, A.; Tang, Y.; Sofroniew, M. V. Astrocytes in Human Central Nervous System Diseases: A Frontier for New Therapies. *Signal Transduct. Target. Ther.* **2023**, *8* (1), 396. https://doi.org/10.1038/s41392-023-01628-9.

(8) Gao, C.; Jiang, J.; Tan, Y.; Chen, S. Microglia in Neurodegenerative Diseases: Mechanism and

Potential Therapeutic Targets. *Signal Transduct. Target. Ther.* **2023**, *8* (1), 359. https://doi.org/10.1038/s41392-023-01588-0.

(9) Bi, W.; Lei, T.; Cai, S.; Zhang, X.; Yang, Y.; Xiao, Z.; Wang, L.; Du, H. Potential of Astrocytes in Targeting Therapy for Alzheimer's Disease. *Int. Immunopharmacol.* **2022**, *113*, 109368. https://doi.org/10.1016/j.intimp.2022.109368.

(10) Nakano-Kobayashi, A.; Canela, A.; Yoshihara, T.; Hagiwara, M. Astrocyte-Targeting Therapy Rescues Cognitive Impairment Caused by Neuroinflammation via the Nrf2 Pathway. *Proc. Natl. Acad. Sci.* **2023**, *120* (33), e2303809120. https://doi.org/10.1073/pnas.2303809120.

(11) Liu, H.; Han, Y.; Wang, T.; Zhang, H.; Xu, Q.; Yuan, J.; Li, Z. Targeting Microglia for Therapy of Parkinson's Disease by Using Biomimetic Ultrasmall Nanoparticles. *J. Am. Chem. Soc.* **2020**, *142* (52), 21730–21742. https://doi.org/10.1021/jacs.0c09390.

(12) Lofts, A.; Abu-Hijleh, F.; Rigg, N.; Mishra, R. K.; Hoare, T. Using the Intranasal Route to Administer Drugs to Treat Neurological and Psychiatric Illnesses: Rationale, Successes, and Future Needs. *CNS Drugs* **2022**, *36* (7), 739–770. https://doi.org/10.1007/s40263-022-00930-4.

(13) Xu, D.; Song, X.-J.; Chen, X.; Wang, J.-W.; Cui, Y.-L. Advances and Future Perspectives of Intranasal Drug Delivery: A Scientometric Review. *J. Controlled Release* **2024**, *367*, 366–384. https://doi.org/10.1016/j.jconrel.2024.01.053.

(14) Chen, Y.; Zhang, C.; Huang, Y.; Ma, Y.; Song, Q.; Chen, H.; Jiang, G.; Gao, X. Intranasal Drug Delivery: The Interaction between Nanoparticles and the Nose-to-Brain Pathway. *Adv. Drug Deliv. Rev.* **2024**, *207*, 115196. https://doi.org/10.1016/j.addr.2024.115196.

(15) Tang, L.; Zhang, R.; Wang, Y.; Liu, M.; Hu, D.; Wang, Y.; Yang, L. Nanoparticle Delivery for Central Nervous System Diseases and Its Clinical Application. *Nano Res.* **2024**, *17* (7), 6305–6322. https://doi.org/10.1007/s12274-024-6598-1.

(16) Rabiee, N.; Ahmadi, S.; Afshari, R.; Khalaji, S.; Rabiee, M.; Bagherzadeh, M.; Fatahi, Y.; Dinarvand, R.; Tahriri, M.; Tayebi, L.; Hamblin, M. R.; Webster, T. J. Polymeric Nanoparticles for Nasal Drug Delivery to the Brain: Relevance to Alzheimer's Disease. *Adv. Ther.* **2021**, *4* (3), 2000076. https://doi.org/10.1002/adtp.202000076.

(17) Kamei, N.; Ikeda, K.; Ohmoto, Y.; Fujisaki, S.; Shirata, R.; Maki, M.; Miyata, M.; Miyauchi, Y.; Nishiyama, N.; Yamada, M.; Ohigashi, Y.; Takeda-Morishita, M. Insulin-Inspired Hippocampal Neuron–Targeting Technology for Protein Drug Delivery. *Proc. Natl. Acad. Sci.* **2024**, *121* (41), e2407936121. https://doi.org/10.1073/pnas.2407936121.

(18) Veys, K.; Fan, Z.; Ghobrial, M.; Bouché, A.; García-Caballero, M.; Vriens, K.; Conchinha, N. V.; Seuwen, A.; Schlegel, F.; Gorski, T.; Crabbé, M.; Gilardoni, P.; Ardicoglu, R.; Schaffenrath, J.; Casteels, C.; De Smet, G.; Smolders, I.; Van Laere, K.; Abel, E. D.; Fendt, S.-M.; Schroeter, A.; Kalucka, J.; Cantelmo, A. R.; Wälchli, T.; Keller, A.; Carmeliet, P.; De Bock, K. Role of the GLUT1 Glucose Transporter in Postnatal CNS Angiogenesis and Blood-Brain Barrier Integrity. *Circ. Res.* **2020**, *127* (4), 466–482. https://doi.org/10.1161/CIRCRESAHA.119.316463.

(19) Anraku, Y.; Kuwahara, H.; Fukusato, Y.; Mizoguchi, A.; Ishii, T.; Nitta, K.; Matsumoto, Y.; Toh, K.; Miyata, K.; Uchida, S.; Nishina, K.; Osada, K.; Itaka, K.; Nishiyama, N.; Mizusawa, H.; Yamasoba, T.; Yokota, T.; Kataoka, K. Glycaemic Control Boosts Glucosylated Nanocarrier Crossing the BBB into the Brain. *Nat. Commun.* **2017**, *8* (1), 1001. https://doi.org/10.1038/s41467-017-00952-3.

(20) Badr, A.; Daily, K. P.; Eltobgy, M.; Estfanous, S.; Tan, M. H.; Chun-Tien Kuo, J.; Whitham, O.; Carafice, C.; Gupta, G.; Amer, H. M.; Shamseldin, M. M.; Yousif, A.; Deems, N. P.; Fitzgerald, J.; Yan, P.; Webb, A.; Zhang, X.; Pietrzak, M.; Ghoneim, H. E.; Dubey, P.; Barrientos, R. M.; Lee, R. J.; Kokiko-Cochran, O. N.; Amer, A. O. Microglia-Targeted Inhibition of miR-17 via Mannose-Coated Lipid Nanoparticles Improves Pathology and Behavior in a Mouse Model of Alzheimer's Disease. *Brain. Behav. Immun.* **2024**, *119*, 919–944. https://doi.org/10.1016/j.bbi.2024.05.006.

(21) Sharma, A.; Porterfield, J. E.; Smith, E.; Sharma, R.; Kannan, S.; Kannan, R. M. Effect of Mannose Targeting of Hydroxyl PAMAM Dendrimers on Cellular and Organ Biodistribution in a Neonatal Brain Injury Model. *J. Controlled Release* **2018**, *283*, 175–189. https://doi.org/10.1016/j.jconrel.2018.06.003.

(22) Lyu, Z.; Peng, L. Potent Drugless Dendrimers. *Nat. Biomed. Eng.* **2017**, *1* (9), 686–688. https://doi.org/10.1038/s41551-017-0136-3.

(23) Kannan, R. M.; Nance, E.; Kannan, S.; Tomalia, D. A. Emerging Concepts in Dendrimer-based Nanomedicine: From Design Principles to Clinical Applications. *J. Intern. Med.* **2014**, *276* (6), 579–617. https://doi.org/10.1111/joim.12280.

(24) Moscariello, P.; Ng, D. Y. W.; Jansen, M.; Weil, T.; Luhmann, H. J.; Hedrich, J. Brain Delivery of Multifunctional Dendrimer Protein Bioconjugates. *Adv. Sci.* **2018**, *5* (5), 1700897. https://doi.org/10.1002/advs.201700897.

(25) Lyu, Z.; Ding, L.; Tintaru, A.; Peng, L. Self-Assembling Supramolecular Dendrimers for Biomedical Applications: Lessons Learned from Poly(Amidoamine) Dendrimers. *Acc. Chem. Res.* **2020**, *53* (12), 2936–2949. https://doi.org/10.1021/acs.accounts.0c00589.

(26) Chen, J.; Zhu, D.; Liu, X.; Peng, L. Amphiphilic Dendrimer Vectors for RNA Delivery: State-of-the-Art and Future Perspective. *Acc. Mater. Res.* **2022**, *3* (5), 484–497. https://doi.org/10.1021/accountsmr.1c00272.

(27) Percec, V.; Wilson, D. A.; Leowanawat, P.; Wilson, C. J.; Hughes, A. D.; Kaucher, M. S.; Hammer, D. A.; Levine, D. H.; Kim, A. J.; Bates, F. S.; Davis, K. P.; Lodge, T. P.; Klein, M. L.; DeVane, R. H.; Aqad, E.; Rosen, B. M.; Argintaru, A. O.; Sienkowska, M. J.; Rissanen, K.; Nummelin, S.; Ropponen, J. Self-Assembly of Janus Dendrimers into Uniform Dendrimersomes and Other Complex Architectures. *Science* **2010**, *328* (5981), 1009–1014. https://doi.org/10.1126/science.1185547.

(28) Liu, X.; Dhumal, D.; Santofimia-Castaño, P.; Liu, J.; Casanova, M.; Garcia-Muñoz, A. C.; Perles-Barbacaru, T.-A.; Elkihel, A.; Zhang, W.; Roussel, T.; Galanakou, C.; Wu, J.; Zerva, E.; Dusetti, N.; Xia, Y.; Liang, X.-J.; Viola, A.; Iovanna, J. L.; Peng, L. Self-Assembling Dendrimer Nanodrug Formulations for Decreased hERG-Related Toxicity and Enhanced Therapeutic Efficacy. *Sci. Adv.* **2025**.

(29) Jiang, Y.; Lyu, Z.; Ralahy, B.; Liu, J.; Roussel, T.; Ding, L.; Tang, J.; Kosta, A.; Giorgio, S.; Tomasini, R.; Liang, X.-J.; Dusetti, N.; Iovanna, J.; Peng, L. Dendrimer Nanosystems for Adaptive Tumor-Assisted Drug Delivery via Extracellular Vesicle Hijacking. *Proc. Natl. Acad. Sci.* **2023**, *120* (7), e2215308120. https://doi.org/10.1073/pnas.2215308120.

(30) Wei, T.; Chen, C.; Liu, J.; Liu, C.; Posocco, P.; Liu, X.; Cheng, Q.; Huo, S.; Liang, Z.; Fermeglia, M.; Pricl, S.; Liang, X.-J.; Rocchi, P.; Peng, L. Anticancer Drug Nanomicelles Formed by Self-Assembling Amphiphilic Dendrimer to Combat Cancer Drug Resistance. *Proc. Natl. Acad. Sci.* **2015**, *112* (10), 2978–2983. https://doi.org/10.1073/pnas.1418494112.

(31) Chen, J.; Zhu, D.; Lian, B.; Shi, K.; Chen, P.; Li, Y.; Lin, W.; Ding, L.; Long, Q.; Wang, Y.; Laurini, E.; Lan, W.; Li, Y.; Tintaru, A.; Ju, C.; Zhang, C.; Pricl, S.; Iovanna, J.; Liu, X.; Peng, L. Cargo-Selective and Adaptive Delivery of Nucleic Acid Therapeutics by Bola-Amphiphilic Dendrimers. *Proc. Natl. Acad. Sci.* **2023**, *120* (21), e2220787120. https://doi.org/10.1073/pnas.2220787120.

(32) Chen, J.; Ellert-Miklaszewska, A.; Garofalo, S.; Dey, A. K.; Tang, J.; Jiang, Y.; Clément, F.; Marche, P. N.; Liu, X.; Kaminska, B.; Santoni, A.; Limatola, C.; Rossi, J. J.; Zhou, J.; Peng, L. Synthesis and Use of an Amphiphilic Dendrimer for siRNA Delivery into Primary Immune Cells. *Nat. Protoc.* **2021**, *16* (1), 327–351. https://doi.org/10.1038/s41596-020-00418-9.

(33) Lyu, Z.; Ralahy, B.; Perles-Barbacaru, T.-A.; Ding, L.; Jiang, Y.; Lian, B.; Roussel, T.; Liu, X.; Galanakou, C.; Laurini, E.; Tintaru, A.; Giorgio, S.; Pricl, S.; Liu, X.; Bernard, M.; Iovanna, J.; Viola, A.; Peng, L. Self-Assembling Dendrimer Nanosystems for Specific Fluorine Magnetic Resonance Imaging and Effective Theranostic Treatment of Tumors. *Proc. Natl. Acad. Sci.* **2024**, *121* (25), e2322403121. https://doi.org/10.1073/pnas.2322403121.

(34) Ding, L.; Lyu, Z.; Perles-Barbacaru, T.; Huang, A. Y.; Lian, B.; Jiang, Y.; Roussel, T.; Galanakou, C.; Giorgio, S.; Kao, C.; Liu, X.; Iovanna, J.; Bernard, M.; Viola, A.; Peng, L. Modular Self-Assembling Dendrimer Nanosystems for Magnetic Resonance and Multimodality Imaging of Tumors. *Adv. Mater.* **2024**, *36* (7), 2308262. https://doi.org/10.1002/adma.202308262.

(35) Garrigue, P.; Tang, J.; Ding, L.; Bouhlel, A.; Tintaru, A.; Laurini, E.; Huang, Y.; Lyu, Z.; Zhang, M.; Fernandez, S.; Balasse, L.; Lan, W.; Mas, E.; Marson, D.; Weng, Y.; Liu, X.; Giorgio, S.; Iovanna, J.; Pricl, S.; Guillet, B.; Peng, L. Self-Assembling Supramolecular Dendrimer Nanosystem for PET Imaging of Tumors. *Proc. Natl. Acad. Sci.* **2018**, *115* (45), 11454–11459. https://doi.org/10.1073/pnas.1812938115.

(36) Shi, Z.; Artemenko, M.; Yu, W.; Zhang, M.; Yi, C.; Chen, P.; Lin, S.; Bian, Z.; Lian, B.; Meng, F.; Chen, J.; Roussel, T.; Li, Y.; Chan, K. K. L.; Ip, P. P. C.; Lai, H.-C.; To, S. K. Y.; Liu, X.; Peng, L.; Wong, A. S. T. Bola-Amphiphilic Dendrimer Enhances Imatinib to Target Metastatic Ovarian Cancer via β-Catenin-HRP2 Signaling Axis. *ACS Appl. Mater. Interfaces* **2025**, *17* (2), 2884–2898. https://doi.org/10.1021/acsami.4c12857.

(37) Liu, X.; Wang, Y.; Chen, C.; Tintaru, A.; Cao, Y.; Liu, J.; Ziarelli, F.; Tang, J.; Guo, H.; Rosas, R.; Giorgio, S.; Charles, L.; Rocchi, P.; Peng, L. A Fluorinated Bola-Amphiphilic Dendrimer for On-Demand Delivery of siRNA, via Specific Response to Reactive Oxygen Species. *Adv. Funct. Mater.* **2016**, *26* (47), 8594–8603. https://doi.org/10.1002/adfm.201604192.

(38) Zeng, H.; Johnson, M. E.; Oldenhuis, N. J.; Tiambeng, T. N.; Guan, Z. Structure-Based Design of Dendritic Peptide Bolaamphiphiles for siRNA Delivery. *ACS Cent. Sci.* **2015**, *1* (6), 303–312. https://doi.org/10.1021/acscentsci.5b00233.

(39) Valentine, D. L. Adaptations to Energy Stress Dictate the Ecology and Evolution of the Archaea. *Nat. Rev. Microbiol.* **2007**, *5* (4), 316–323. https://doi.org/10.1038/nrmicro1619.

(40) Zhang, W.; Dhumal, D.; Zhu, X.; Ralahy, B.; Ellert-Miklaszewska, A.; Wu, J.; Laurini, E.; Yao, Y.; Kao, C.; Iovanna, J. L.; Pricl, S.; Kaminska, B.; Xia, Y.; Peng, L. Bola-Amphiphilic Glycodendrimers: New Carbohydrate-Mimicking Scaffolds to Target Carbohydrate-Binding Proteins. *Chem. – Eur. J.* **2022**, *28* (58), e202201400. https://doi.org/10.1002/chem.202201400.

(41) Lundquist, J. J.; Toone, E. J. The Cluster Glycoside Effect. *Chem. Rev.* **2002**, *102* (2), 555–

View Article Online
DOI: 10.1039/D5NR03017J

578. https://doi.org/10.1021/cr000418f.

(42) Su, L.; Feng, Y.; Wei, K.; Xu, X.; Liu, R.; Chen, G. Carbohydrate-Based Macromolecular Biomaterials. *Chem. Rev.* **2021**, *121* (18), 10950–11029. https://doi.org/10.1021/acs.chemrev.0c01338.

(43) Rodrigo, A. C.; Bromfield, S. M.; Laurini, E.; Posocco, P.; Pricl, S.; Smith, D. K. Morphological Control of Self-Assembled Multivalent (SAMul) Heparin Binding in Highly Competitive Media. *Chem. Commun.* **2017**, *53* (47), 6335–6338. https://doi.org/10.1039/C7CC02990J.

(44) Garrigue, P.; Tang, J.; Ding, L.; Bouhlel, A.; Tintaru, A.; Laurini, E.; Huang, Y.; Lyu, Z.; Zhang, M.; Fernandez, S.; Balasse, L.; Lan, W.; Mas, E.; Marson, D.; Weng, Y.; Liu, X.; Giorgio, S.; Iovanna, J.; Pricl, S.; Guillet, B.; Peng, L. Self-Assembling Supramolecular Dendrimer Nanosystem for PET Imaging of Tumors. *Proc. Natl. Acad. Sci.* **2018**, *115* (45), 11454–11459. https://doi.org/10.1073/pnas.1812938115.

(45) Ding, L.; Lyu, Z.; Louis, B.; Tintaru, A.; Laurini, E.; Marson, D.; Zhang, M.; Shao, W.; Jiang, Y.; Bouhlel, A.; Balasse, L.; Garrigue, P.; Mas, E.; Giorgio, S.; Iovanna, J.; Huang, Y.; Pricl, S.; Guillet, B.; Peng, L. Surface Charge of Supramolecular Nanosystems for In Vivo Biodistribution: A MicroSPECT/CT Imaging Study. *Small* **2020**, *16* (37), 2003290. https://doi.org/10.1002/smll.202003290.

(46) Cong, M.; Xu, G.; Yang, S.; Zhang, J.; Zhang, W.; Dhumal, D.; Laurini, E.; Zhang, K.; Xia, Y.; Pricl, S.; Peng, L.; Zhao, W. A Self-Assembling Prodrug Nanosystem to Enhance Metabolic Stability and Anticancer Activity of Gemcitabine. *Chin. Chem. Lett.* **2022**, *33* (5), 2481–2485. https://doi.org/10.1016/j.cclet.2021.11.083.

(47) Hammond, T. R.; Dufort, C.; Dissing-Olesen, L.; Giera, S.; Young, A.; Wysoker, A.; Walker, A. J.; Gergits, F.; Segel, M.; Nemesh, J.; Marsh, S. E.; Saunders, A.; Macosko, E.; Ginhoux, F.; Chen, J.; Franklin, R. J. M.; Piao, X.; McCarroll, S. A.; Stevens, B. Single-Cell RNA Sequencing of Microglia throughout the Mouse Lifespan and in the Injured Brain Reveals Complex Cell-State Changes. *Immunity* **2019**, *50* (1), 253-271.e6. https://doi.org/10.1016/j.immuni.2018.11.004.

(48) Li, Q.; Cheng, Z.; Zhou, L.; Darmanis, S.; Neff, N. F.; Okamoto, J.; Gulati, G.; Bennett, M. L.; Sun, L. O.; Clarke, L. E.; Marschallinger, J.; Yu, G.; Quake, S. R.; Wyss-Coray, T.; Barres, B. A. Developmental Heterogeneity of Microglia and Brain Myeloid Cells Revealed by Deep Single-Cell RNA Sequencing. *Neuron* **2019**, *101* (2), 207-223.e10. https://doi.org/10.1016/j.neuron.2018.12.006.

View Article Online
DOI: 10.1039/D5NR03017J

Data Availability Statement

All data generated in this study are included in the article and the supplementary materials.

Ling PENG